Journal of Alloys and Compounds 705 (2017) 462–467

Contents lists available at ScienceDirect

Journal of Alloys and Compounds

journal homepage: http://www.elsevier.com/locate/jalcom

Investigation of amorphous phase formation in Fe-Co-Si-B-P - Thermodynamic analysis and comparison between mechanical alloying and rapid solidification experiments

M. Imani*, M.H. Enayati

Department of Materials Engineering, Isfahan University of Technology, Isfahan, 84156-83111, Iran

ARTICLE INFO

Article history:
Received 5 January 2017
Received in revised form
7 February 2017
Accepted 10 February 2017
Available online 14 February 2017

Keywords:
Glass forming ability
Mechanical alloying
Iron-base amorphous alloys
Extended Miedema model

ABSTRACT

In recent years, amorphous alloys have received a considerable attraction because of their physical, mechanical and magnetic properties. Fe-Co alloy system has good soft magnetic properties (high magnetic saturation and high Curie point) which makes it suitable for high temperature magnetic applications. In this paper, the effect of different elements on glass forming ability (GFA) of Fe-Co system was evaluated based on Meidema semi-empirical model and the results were compared to mechanical alloying (MA) experiments. Si, B and P seem to be good elements to be added to Fe-Co alloys with respect to thermodynamics and kinetics requirements. Calculations based on extended Miedema model showed that enthalpy and Gibbs free energy changes for solid state amorphisation of $Fe_{70}Co_7Si_8B_8P_7$ were −179 (kJ mol^{-1}) and −181 (kJ mol^{-1}) respectively, but MA experiments in three different routes did not lead to amorphisation in this system. Also comparison between MA and melt spinning (MS) techniques showed GFA in both techniques are completely different.

1. Introduction

Metallic amorphous alloys are advanced materials that have interesting combination of physical, chemical, mechanical, and magnetic properties which cannot be obtained in conventional crystalline alloys [1]. These unique characteristics make them attractive for a variety of applications. The ability of producing nano-crystalline alloys with high controllability from crystallization of amorphous phase, is another importance of amorphous materials. Consequently there has been a lot of interest in understanding the structure, forming ability and properties of these materials [2]. In general, there are several methods for fabrication of amorphous alloys among which rapid solidification process (RSP) and mechanical alloying (MA) are more important than others. In recent years, progression and development trends in the field of amorphous alloys have been toward to alloy systems such as Iron-based amorphous alloy with high performance while having low cost [1]. Among the many Iron-based amorphous alloys, Fe—Co alloys have a special importance due to their interesting soft magnetic properties such as high magnetization saturation [3] and also high Curie temperature [4] that making them suitable for the high temperature applications such as new generation turbine engines and recording media [5–7]. For these applications good mechanical properties are also important. A combination of good mechanical properties beside good soft magnetic properties is a challenge for soft magnetic materials which can be achieved in amorphous state. Fe-Co alloys in amorphous state keep their good soft magnetic properties with a high value of in yield strength (~4000 MPa) [1,8]. Amorphous Fe-Co based alloys were synthesized by RSP process successfully [1,9] but MA amorphisation of Fe-Co alloys seems to be difficult due to the small negative heat of mixing (−2 kJ/mol) and low mutual solubility at room temperature [10,11]. However MA amorphisation in Fe-Co alloys can be improved by adding suitable elements [12,13]. Based on experimental evidence, two criteria for the solid-state amorphisation reaction are developed; A large negative heat of mixing, ΔH_{mix}, between alloying elements as well as a large difference between diffusion coefficient of one element in the others [14]. The latter is attained where there is a large difference in atomic size elements. In the present paper, the effect of addition of different metalloid elements on amorphisation of Fe-Co system was investigated. The amorphisation ability was predicted based on thermodynamic analysis (thermodynamic criteria) by Miedema's semi-empirical model [15] and atomic size mismatch (kinetic criteria). The

* Corresponding author.
E-mail address: moein.imani@ma.iut.ac.ir (M. Imani).

http://dx.doi.org/10.1016/j.jallcom.2017.02.100
0925-8388/

amorphous phase formation enthalpy and Gibbs free energy change were calculated based on Extended Miedema's model [16]. The results were compared with those obtained by mechanical alloying process. Finally there is also comparison between MA and MS techniques experiments in Fe-Co-Si-B-P alloy system.

2. Materials and methods

Mixture of Iron (Fe), Cobalt (Co), Silicone (Si), Boron (B) and phosphorous (P) powders with $Fe_{70}Co_7Si_8B_8P_7$ composition were MAed in a high energy planetary ball mill (Fritsch P7) at room temperature. Table 1 shows the characteristics of raw materials. The vial was hardened chromium steel with 120 ml volume and balls were hardened high carbon steel with three different size of 10 (#5), 15 (#6) and 18 mm (#2). Ball to powder weight ratio and rotation speed were 10:1 and 320 rpm respectively. In order to avoid oxidation, MA process was carried out under Ar atmosphere. Phase analysis was performed using X-ray diffractometer (Philips XPERT-MPD) with Cu Kα radiation (λ = 0.1542 nm), time per step of 0.05 s at 2Θ = 10-100°. MA was performed in three different routes as demonstrated in Table 2. Miedema's Extended model was used to calculate the enthalpy and Gibbs free energy change of amorphisation in $Fe_{70}Co_7Si_8B_8P_7$ alloy system.

3. Results and discussion

3.1. Selection of suitable elements based on mixing enthalpy (ΔH_{mix}) and atomic size mismatch

ΔH_{mix} was calculated using Miedema's semi-empirical model [15] to find which element can produce a negative ΔH_{mix}, required for MA amorphisation with Fe in solid state. The Gibbs free energy change (ΔG) can be expressed as:

$$\Delta G = \Delta H - T\Delta S \quad (1)$$

where ΔH is mixing enthalpy change, T, ambient temperature and ΔS is mixing entropy change. For a binary ideal solid solutions ΔS can be written as:

$$\Delta S = -R(X_A \ln X_A + X_B \ln X_B) \quad (2)$$

$$X_A + X_B = 1$$

where R is universal gas constant and X_A and X_B are atomic concentrations in solid solution.

According to Miedema's semi-empirical model the heat of mixing in A-B system is due to the, electronegativity difference (a negative term) and electron density difference (a positive term) between two components. In Miedema's semi-empirical model, ΔH_{AB}, includes three parts:

$$\Delta H_{total} = \Delta H_{Chemical} + \Delta H_{Elastic} + \Delta H_{Structural} \quad (3)$$

where $\Delta H_{Chemical}$ is chemical enthalpy, $\Delta H_{Elastic}$, elastic enthalpy and $\Delta H_{Structural}$, structural enthalpy.

Table 1
Characteristics of raw materials.

Raw materials	Purity (%)	Particle size (μm)	Structure
Fe	99.00	<100	Crystalline
Co	99.8	<50	Crystalline
Si	99.9	<50	Crystalline
B	99.9	<30	Crystalline
P	98	<30	Amorphous

Table 2
MA routes.

Routes	Explains
Route A	Continuous MA for 160 h
Route B	MA with stearic acid as a process control agent (PCA) for 100 h
Route C	MA for 50 h + annealing at 800 °C for 1 h + further MA for 60 h

The chemical contribution is due to difference in bonding energy of atoms of components in the initial and mixing states. $\Delta H_{Elastic}$ and $\Delta H_{Structural}$ contributions are due to atomic size difference and the difference in valence electrons and crystal structure of solvent and solute atoms, respectively. The chemical contribution of ΔH_{total} is calculated as follow:

$$\Delta H_{AB}^{(Chemical)} = X_A X_B \left[f_A^B \, \Delta H_{B\ in\ A}^{(Sol.)} + f_B^A \, \Delta H_{A\ in\ B}^{(Sol.)} \right] \quad (4)$$

f_A^B, f_B^A and $\Delta H_{B\ in\ A}^{(Sol.)}$ are the concentration function and solution enthalpy for mixing B in A respectively that defined as:

$$f_A^B = X_A^S \left[1 + \gamma \left(X_A^S X_B^S \right)^2 \right] \quad (5)$$

$$f_B^A = X_B^S \left[1 + \gamma \left(X_A^S X_B^S \right)^2 \right] \quad (6)$$

$$\Delta H_{B\ in\ A}^{(Sol.)} = \left[\frac{V_A^{\frac{2}{3}}}{\left(n_{ws}^{-\frac{1}{3}} \right)_{av}} \right] \left\{ -p(\Delta\phi^*)^2 + Q \left(\Delta n_{ws}^{\frac{1}{3}} \right) - R^* \right. \quad (7)$$

Also X_A^S and X_B^S defined as:

$$X_A^S = \frac{X_A V_A^{\frac{2}{3}}}{X_A V_A^{\frac{2}{3}} + X_B V_B^{\frac{2}{3}}} \quad (8)$$

$$X_B^S = \frac{X_B V_B^{\frac{2}{3}}}{X_A V_A^{\frac{2}{3}} + X_B V_B^{\frac{2}{3}}} \quad (9)$$

where V is the molar volumes of atoms, ϕ^* is the work function of B, n_{ws} is the electron density, P, Q and R^* are empirical constants and γ is 0 for solid solution, 5 for amorphous phase and 8 for intermetallic compound. R^* can be calculated from existing data [17–19]. P equal 14.2 and 10.7 transition and non-transition metals respectively. It should be noted that P/Q = 9.4 and R^* is taken in account only for those systems which include one transition metals and non-transition metals. The required parameters for calculations of thermodynamics values are shown in Table 3. Phosphorus parameters are extended from Ref. [18]. Solution enthalpy of some elements in Iron and atomic size mismatch are shown in Tables 4 and 5 respectively.

According to Tables 4 and 5, the negative heat of mixing of Co with Fe (−2 kJ/mol) and the small mismatch between their atomic radii and electronegativity make the formation of Fe-Co alloys easy and feasible in MA. Many researches showed that formation of Fe-Co alloys in wide any range of Co (10–90 wt%) easily and in a short time in MA [20]. According to values given in Tables 4 and 5, Zr, Ti, Al, Nb, Si, B, P and C have required thermodynamics and kinetic values to be add to Fe-Co alloys for successful amorphisation. In contrast elements such as Cu, La and Hf because of their positive heat of mixing with Fe attend to

Table 3
The required parameters for calculation of thermodynamics values [15].

Metal	ϕ^* (V)	$n_{ws}^{1/3}$ ($(d.u.)^{1/3}$)	$V_m^{2/3}$ (cm^2)
Fe	4.93	1.77	3.7
Co	5.10	1.75	3.5
Cr	4.65	1.73	3.7
Ni	5.20	1.75	3.5
Zr	3.40	1.39	5.8
Nb	4.00	1.62	4.9
Mo	4.65	1.77	4.4
Ti	3.65	1.47	4.8
V	4.25	1.64	4.1
Cu	4.55	1.47	3.7
Mn	4.45	1.61	3.8
W	4.80	1.81	4.5
Al	4.20	1.39	4.6
Y	3.20	1.21	7.3
Ta	4.05	1.63	4.9
La	3.05	1.09	8.0
Hf	3.55	1.43	5.6
Si	4.70	1.50	4.2
B	4.75	1.55	2.8
P	5.55	1.65	4.15
C	6.20	1.90	1.8

Table 4
Solution enthalpy of some elements in Iron based on Miedema's semi-empirical model (kJ/mole).

	Co	Cr	Ni	Zr	Nb	Mo	Ti	V	Cu	Mn	W	Al	Ta	La	Hf	Y	Si	B	C	P
Fe	−2	−5.7	−6	−125	−76	−8	−86	−30	+58	+0.9	−0.2	−95	−70	+123	+15	−6	−123	−84	−82	−233

Table 5
Atomic radii and atomic size mismatch ($(R_M\text{-}R_{Fe})/R_{Fe}$).

Element	Fe	Co	Cr	Ni	Zr	Nb	Mo	Ti	V	Cu	Mn	W	Al	Ta	La	Hf	Y	Si	B	C	P
Atomic radios (pm)	126	125	128	124	160	146	139	147	134	128	127	139	143	146	187	159	180	111	90	70	128
atomic size mismatch (%)	–	0.8	1.5	1.5	26.9	15.8	10.3	16.6	6.3	1.5	0.8	10.3	13.4	15.8	48.4	26.1	42.8	11.9	28.5	44.4	1.6

segregate and are not suitable choice for amorphisation. Yet another important criteria is that alloying elements in Fe-Co system, should not lower good magnetic properties of Fe-Co alloys such as high curie point and low coercively. Therefore although Zr has good thermodynamics and kinetical values, but it reduces the curie temperature of Fe-Co alloys [21–23]. As a result; only three elements; Si, B and P were selected. Many researchers reported that the best GFA is obtained where 20–25 at. % metalloid elements exist beside metallic elements [2,24] thus $Fe_{70}Co_7Si_8B_8P_7$ alloy system was chosen in this study. Fe-Co-Si-B-P alloy system has been amorphized by melt spinning process by Liu et al. at Caltech [9] but there is no report on amorphisation by MA technique.

3.2. Gibbs free energy and enthalpy changes of amorphisation for $Fe_{70}Co_7Si_8B_8P_7$ alloy system

In a ternary alloy system as shown in Eq. (10), only the binary interactions between components are considered [16]. The enthalpy change for the formation of A-B-C ternary alloy is given by Refs. [17,25]. Similar to Medima's semi-empirical model, ΔH_{total} is due to the chemical, elastic and structural enthalpies:

$$\Delta H_{ABC} = \Delta H_{AB} + \Delta H_{AC} + \Delta H_{BC} \quad (10)$$

$$\Delta H_{total} = \Delta H_{Chemical} + \Delta H_{Elastic} + \Delta H_{Structural} \quad (11)$$

$$\Delta H_{ABC}^{Chemical} = \Delta H_{AB}^{Chemical} + \Delta H_{AC}^{Chemical} + \Delta H_{BC}^{Chemical} \quad (12)$$

$$\Delta H_{ABC}^{Elastic} = \Delta H_{AB}^{Elastic} + \Delta H_{AC}^{Elastic} + \Delta H_{BC}^{Elastic}$$

$$\Delta H_{ABC}^{Structural} = \Delta H_{AB}^{Structural} + \Delta H_{AC}^{Structural} + \Delta H_{BC}^{Structural} \quad (13)$$

The amorphous structures have two components; topological and chemical disorder [26]. The topological disorder is from lack of repeatable geometric packing. The chemical disorder is caused by the local environment of each atoms. For amorphous phase, elastic and structural enthalpy changes are negligible because there is no crystalline structure and ordering. Mixing enthalpy for an amorphous alloy defined as:

$$\Delta H^{Amorphous} = \Delta H^{Chemical} + 3.5\sum(X_i T_{m,i} + X_j T_{m,j}) \quad (14)$$

$3.5\sum(X_i T_{m,i} + X_j T_{m,j})$ is topological disorder in the amorphous state and is estimated by Miedema. Some evidences show that the Miedema extended model can be successfully applied to five-elements (quinary) alloy system [27]. The calculated enthalpy and Gibbs free energy changes for amorphisation of $Fe_{70}Co_7Si_8B_8P_7$ were −179 ($kJ.mole^{-1}$) and −181 ($kJ.mole^{-1}$) respectively.

3.3. Structural changes in $Fe_{70}Co_7Si_8B_8P_7$ alloy system in three different routes during MA

3.3.1. Route A

Fig. 1 show X-ray diffraction (XRD) patterns of $Fe_{70}Co_7Si_8B_8P_7$ alloy system during MA. After 160 h MA, no amorphous phase was formed instead an α-Fe solid solution containing Co, Si, B and P with body centered cubic (BCC) crystalline structure developed.

3.3.2. Route B

Severe adhesion of powders on balls and vial surfaces was observed in route A. This can significantly reduce the milling efficiency and limits the impact energy of colliding balls, hindering the amorphisation reaction. In route B stearic acid was used (1.5 wt%) to control the cold welding of metallic powders. Reports show existence of PCAs during MA has considerable effects on structural changes [28,29]. Fig. 2 shows XRD pattern of $Fe_{70}Co_7Si_8B_8P_7$ after 100 h MA with stearic acid (1.5 wt%) as PCA. As seen no amorphous structure was formed.

3.3.3. Route C

In some alloy systems MA amorphisation starts with formation of an intermetallic compound(s) which transform to amorphous structure upon further milling [13]. Therefore intermediate annealing could help amorphisation by formation of intermetallic compound(s) at layers interfaces. Fig. 3 shows XRD patterns of $Fe_{70}Co_7Si_8B_8P_7$ after annealing. Small peaks between 40 and 45° are related to some unknown intermetallic phases. Further milling of annealed powder for 60 h did not lead to amorphisation which is in contrast to thermodynamics calculation given in previous section. The lack of amorphisation in Fe–Co system can be caused a small negative heat of mixing (−2 kJ/mol) of Fe-Co at room temperature. Therefore, Fe-Co alloy favorably form a supersaturated solid solution under MA condition in which Si, B and P are also dissolved.

3.4. Comparison between RSP and MA

Liu et al. in Caltech group [9] investigated GFA in Fe-Co-Si-B-P alloy systems by melt spinning technique. Their experiments showed the best GFA in Fe-Co-Si-B-P alloy system reached where metallic elements (Fe and Co) are 77 at.% and Si, B and P are 8,8 and 7 at.% respectively. They also showed from phase diagrams that the eutectic points appear to have similar Si and B atomic percentages. Thus $Fe_{70}Co_7Si_{8.5}B_{7.5}P_7$ alloy system is around eutectics point of Fe-Si-B and Co-Si-B ternary phase diagrams and $Fe_{70}Co_7Si_{8.5}B_{7.5}P_7$ alloy system is an optimum compositions for achieving amorphous structure by RSP techniques. In contrast, many researches show GFA of a constant composition in RSP and MA techniques are different [30]. In the case of RSP, the best composition for amorphisation is around eutectic point. In contrast, in the case of MA, GFA is the highest where a large number of intermetallic compounds forms in alloy system [13]. Intermetallic compounds are usually in the center of phase diagrams. Thus in MA, the formation amorphous phase is more probable when elements are in equiatomic percentage. Presence of intermetallic compounds in alloy systems could help amorphisation by two ways. First, intermetallic compounds like A_mB_n typically have a complex crystal structure and formation of A_mB_n intermetallic compound requires diffusion of both A and B atoms which is not possible under MA conditions while formation of amorphous phase requires the diffusion of only one elements. Second reason is related to energetic parameters. The free energy change of the crystalline to amorphous transformation is typically about 5–20 kJ mol^{-1} [31]. MA is associated with heavy plastic deformation and therefore, a high density of defects such as dislocation, grain boundaries, stacking faults and antiphase boundaries, etc.. It is believed that the rate creation of defect during MA controls the kinetics of amorphisation [31]. Intermetallic compounds have a narrow composition range, a slight deviation from stoichiometry can sharply increases the free energy of the system. This behavior is also explained as anti-site disordering. The relative effect of different defects on raising the free energy of the system are shown in Table 6 [31–33].

From Table 6, it can be concluded that for intermetallics grain boundaries and disordering have dominant effect [34]. When the free energy of system becomes higher than that for a hypothetical amorphous phase, the crystalline phase destabilizes and amorphisation is thermodynamically favored. In contrast for a solid solution, the only defects that can be introduced into the system during milling are dislocations and grain boundaries. The excess free energy from these defects is considerably lower than that for an intermetallic compound. Therefore, crystalline to amorphous phase transition becomes thermodynamically more

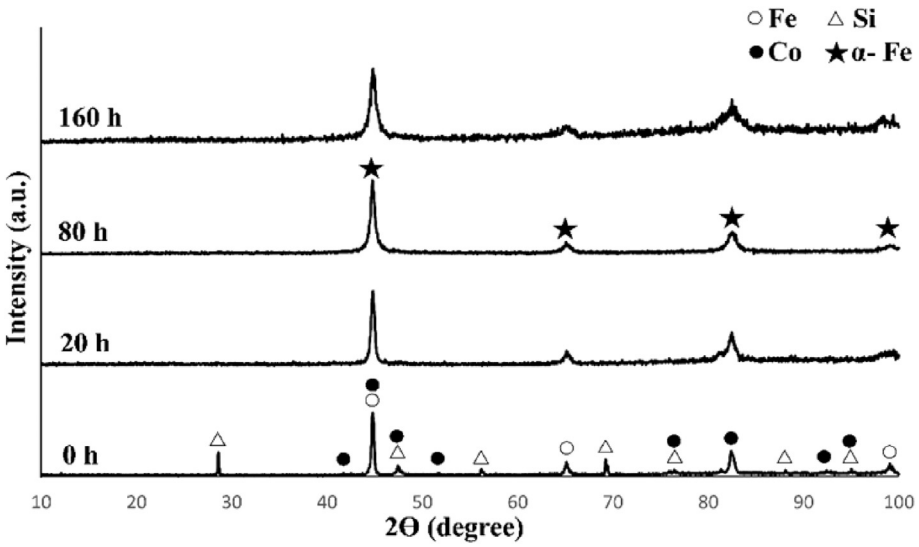

Fig. 1. XRD patterns of $Fe_{70}Co_7Si_8B_8P_7$ at different MA times.

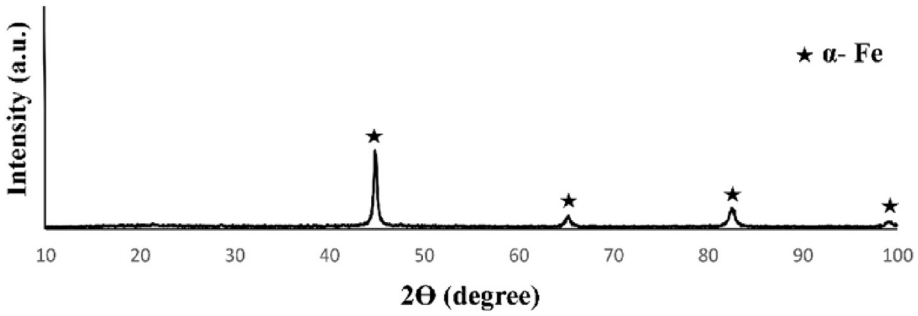

Fig. 2. XRD pattern of $Fe_{70}Co_7Si_8B_8P_7$ after 100 h MA with stearic acid as PCA (1.5 wt%).

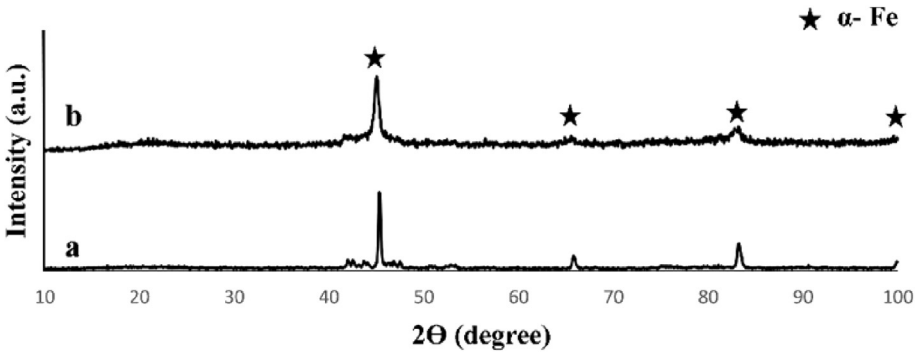

Fig. 3. XRD patterns a) after annealing of 50 h milled powder, b) after further milling of annealed powder for 60 h.

Table 6
Effect of different defects on the free energy of the system.

Type of defect	Maximum free energy (kJ/mole of atoms)
Dislocation ($10^{16}/m^2$)	1
Grain size (1 nm)	10
Disordering (anti-site disordering)	12
Vacancies (1%)	1

difficult [33]. Sharma et al. [35] studied MA amorphisation in $Fe_{42}X_{28}Zr_{10}B_{20}$ (where X = Al, Co, Ge, Mn, Ni, and Sn) alloy. They showed in presence of Al and Ni, because of existance of 10 intermetallic compounds, amorphisation achieved in MA. In contrast in alloys containing Co, Mn and Sn wide solid solution exists therefore amorphous phase did not form. Similar results were reported by Liu et al. [12]. They showed for Fe-Co-Ni-Zr-B alloy system, full amorphous phase was not achieved by MA. In Fe-Co-Si-B-P alloy there are 21 intermetallics compound between each binary system. Although the presence of a wide solid solution in Fe-Co phase diagram prevents amorphisation reaction in MA.

4. Conclusions

Thermodynamic calculations based on Miedema's extended model showed formation enthalpy changes and Gibbs free energy for amorphisation of $Fe_{70}Co_7Si_8B_8P_7$ alloy system are −179 kJ mol^{-1} and -181 kJ mol^{-1}, respectively. These calculations show there is sufficient thermodynamics and kinetics tendency for MA amorphisation in $Fe_{70}Co_7Si_8B_8P_7$ alloy system. In spite of this prediction, MA of $Fe_{70}Co_7Si_8B_8P_7$ alloy in three different routes did not lead to amorphous phase. This is probably due to the presence of wide solid solution in Fe-Co phase diagram.

Acknowledgements

This research did not receive any specific grant from funding agencies in the public, commercial, or not-for-profit sectors.

References

[1] C. Suryanarayana, A. Inoue, Iron-based bulk metallic glasses, Int. Mater. Rev. 58 (2013) 131–166.
[2] C. Suryanarayana, A. Inoue, Bulk Metallic Glasses, CRC Press, 2010.
[3] T. Sourmail, Near equiatomic FeCo alloys: constitution, mechanical and magnetic properties, Prog. Mater. Sci. 50 (2005) 816–880.
[4] H. Shokrollahi, The magnetic and structural properties of the most important alloys of iron produced by mechanical alloying, Mater. Des. 30 (2009) 3374–3387.
[5] J. Filipecki, Z. Mandecki, C. Conde, A. Conde, Crystallization of (Fe, Co) 78Si9B13 alloys: influence of relaxation processes, J. Mater. Sci. 33 (1998) 2171–2177.
[6] N. Poudyal, C. Rong, Y. Zhang, D. Wang, M. Kramer, R.J. Hebert, et al., Self-nanoscaling in FeCo alloys prepared via severe plastic deformation, J. Alloys Compd. 521 (2012) 55–59.
[7] M. Yousefi, S. Sharafi, A. Mehrolhosseiny, Correlation between structural parameters and magnetic properties of ball milled nano-crystalline Fe–Co–Si powders, Adv. Powder Technol. 25 (2014) 752–760.
[8] A. Inoue, B. Shen, C. Chang, Super-high strength of over 4000 MPa for Fe-based bulk glassy alloys in [(Fe 1– x Co x) 0.75 B 0.2 Si 0.05] 96 Nb 4 system, Acta Mater. 52 (2004) 4093–4099.
[9] X. Liu, A Study on Iron-based Amorphous Alloys: Alloy Development, Thermodynamics and Soft Magnetism (PhD thesis dissertation), California Institute of Technology, 2014.
[10] H. Laala-Bouali, F.-Z. Bentayeb, S. Louidi, X. Guo, S. Tria, J. Suñol, et al., X-ray line profile analysis of the ball-milled Fe–30Co alloy, Adv. Powder Technol. 24 (2013) 168–174.
[11] R. Satthawong, N. Koizumi, C. Song, P. Prasassarakich, Bimetallic Fe–Co catalysts for CO 2 hydrogenation to higher hydrocarbons, J. CO2 Util. 3 (2013) 102–106.
[12] Y. Liu, I. Chang, P. Bowen, Amorphization and microstructural evolution in multicomponent (FeCoNi) 70 Zr 10 B 20 alloy system by mechanical alloying, Mater. Sci. Eng. A 304 (2001) 389–393.
[13] S. Sharma, R. Vaidyanathan, C. Suryanarayana, Criterion for predicting the glass-forming ability of alloys, Appl. Phys. Lett. 90 (2007) 1915.
[14] M. Enayati, F. Mohamed, Application of mechanical alloying/milling for

synthesis of nanocrystalline and amorphous materials, Int. Mater. Rev. 59 (2014) 394–416.
[15] A. Miedema, P. De Chatel, F. De Boer, Cohesion in alloys—fundamentals of a semi-empirical model, Phys. B+ C 100 (1980) 1–28.
[16] A. Goncalves, M. Almeida, Extended Miedema model: predicting the formation enthalpies of intermetallic phases with more than two elements, Phys. B Condens. Matter 228 (1996) 289–294.
[17] Z. Adabavazeh, F. Karimzadeh, M. Enayati, Thermodynamic analysis of (Ni, Fe) 3 Al formation by mechanical alloying, J. Chem. Thermodyn. 54 (2012) 406–411.
[18] A. d. Niessen, F. De Boer, R. Boom, P. De Chatel, W. Mattens, A. Miedema, Model predictions for the enthalpy of formation of transition metal alloys II, Calphad 7 (1983) 51–70.
[19] P. Ray, M. Akinc, M. Kramer, Applications of an extended Miedema's model for ternary alloys, J. Alloys Compd. 489 (2010) 357–361.
[20] F. Sánchez-De Jesús, A. Bolarín-Miró, C. Cortés Escobedo, G. Torres-Villaseñor, P. Vera-Serna, Structural analysis and magnetic properties of FeCo alloys obtained by mechanical alloying, J. Metall. 2016 (2016).
[21] L. Kiss, G. Huhn, T. Kemeny, J. Balogh, D. Kaptas, Magnetic properties of FeZr metastable phases, J. Magn. Magn. Mater. 160 (1996) 229–232.
[22] H. Okamoto, Fe-Zr (iron-zirconium), J. phase Equilibria 14 (1993) 652–653.
[23] F. Stein, G. Sauthoff, M. Palm, Experimental determination of intermetallic phases, phase equilibria, and invariant reaction temperatures in the Fe-Zr system, J. Phase Equilibria 23 (2002) 480–494.
[24] M. Madinehei, Improvement of Corrosion and Mechanical Properties of Amorphous Steels by Microalloying and Nanocrystallization, 2015.
[25] E. Dastanpoor, M. Enayati, F. Karimzadeh, Synthesis of Cu–Zr–Al/Al2O3 amorphous nanocomposite by mechanical alloying, Adv. Powder Technol. 25 (2014) 519–523.
[26] R. Babilas, R. Nowosielski, Iron-based bulk amorphous alloys, Arch. Mater. Sci. Eng. 44 (2010) 5–27.
[27] F. Salemi, M. Abbasi, F. Karimzadeh, Synthesis and thermodynamic analysis of nanostructured CuNiCoZnAl high entropy alloy produced by mechanical alloying, J. Alloys Compd. 685 (2016) 278–286.
[28] B.V. Neamţu, T.F. Marinca, H.F. Chicinaş, I. Chicinaş, O. Isnard, Effect of process control agents on the FeSiB powder amorphisation by wet mechanical alloying, in: Advanced Engineering Forum, 2015, pp. 37–41.
[29] M. Pilar, J. Sunol, J. Bonastre, L. Escoda, Influence of process control agents in the development of a metastable Fe–Zr based alloy, J. Non Crystalline Solids 353 (2007) 848–850.
[30] B. Murty, M.M. Rao, S. Ranganathan, Differences in the glass-forming ability of rapidly solidified and mechanically alloyed Ti-Ni-Cu alloys, Mater. Sci. Eng. A 196 (1995) 237–241.
[31] M. Swanson, J. Parsons, C. Hoelke, J. Corbett, G. Watkins, Radiation Effects in Semiconductors, Gordon and Breach, New York, 1971, p. 359.
[32] Y. Cho, C. Koch, Mechanical milling of ordered intermetallic compounds: the role of defects in amorphization, J. Alloys Compd. 194 (1993) 287–294.
[33] C. Suryanarayana, Mechanical Alloying and Milling, CRC Press, 2004.
[34] F. Froes, C. Suryanarayana, K. Russell, C. Ward-Close, Far from equilibrium processing of light metals, Nov. Tech. Synthesis Process. Adv. Mater. (1995).
[35] S. Sharma, Amorphous Phase Formation in Mechanically Alloyed Iron-based Systems: ProQuest, 2008.